

# Bifurcations of relative equilibria of an oblate gyrostat with a discrete damper

Ralph A. Sandfry · Christopher D. Hall

Received: 6 May 2005 / Accepted: 18 May 2006 / Published online: 19 August 2006  
© Springer Science + Business Media B.V. 2006

**Abstract** We investigate relative equilibria of an oblate gyrostat with a discrete damper. Linear and nonlinear methods yield stability conditions for simple spins about the nominal principal axes. We use analytical and numerical methods to explore other equilibria, including bifurcations that occur for varying rotor momentum and damper parameters. These bifurcations are complex structures that are perturbations of the zero rotor momentum case. We use Lyapunov–Schmidt reduction to determine an analytic relationship between parameters to determine conditions for which a jump phenomenon occurs.

**Keywords** Bifurcation · Continuation · Gyrostat

## 1 Introduction

The equilibria and stability of spinning satellites have received considerable attention since the initial experiences of Explorer I [10]. Destabilized by energy

dissipation, Explorer I's loss was followed by considerable efforts to sharpen the stability conditions for spinning satellites in the presence of damping. A gyrostat model, consisting of a rigid body with an axisymmetric rotor, has often been used to study the dynamics of satellites with a single rotor [2, 5, 8, 9, 11]. The most commonly studied equilibrium state is the nominal spin, where the satellite spin-axis is aligned with the axisymmetric rotor spin-axis. Much work has been focused on the stability of the nominal spin in the presence of energy dissipation. However, when the nominal spin is destabilized other possible stable equilibria exist. These equilibria represent potential trap states which could capture the free-spinning satellite until a correcting maneuver is performed. These alternative equilibria may include other principal-axis spins as well as off-axis spins within principal planes. Of particular significance is the potential jump from the nominal spin to another stable equilibria should stability be lost.

We study the multiple equilibria of a free-spinning oblate gyrostat with a spring-mass damper. The gyrostat is free of external forces, external torques and rotor torque. The equilibria depend on the values of a number of system parameters, such as spring stiffness, damper location or rotor momentum. Numerical and analytical methods are used to determine bifurcation branches and key points in parameter space. The primary tool is numerical continuation, including two-parameter continuation to explore the behavior of multiple equilibria in parameter space. We focus on the branching

---

This paper is declared a work of the U.S. Government and is not subject to copyright protection in the United States

---

R. A. Sandfry (✉)  
United States Air Force Academy, Colorado, CO 80840,  
USA  
e-mail: ralph.sandfry@usafa.af.mil

C. D. Hall  
Virginia Polytechnic Institute and State University,  
Blacksburg, VA 24061, USA

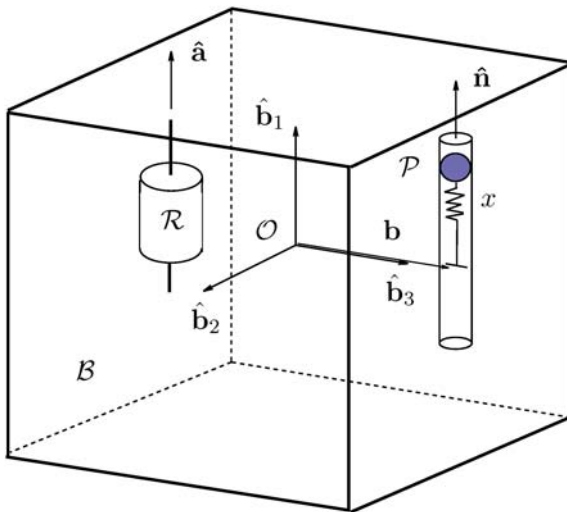


**Fig. 1** Single-rotor axial gyrostat with aligned discrete damper

behavior of the nominal spin and turning points in a principal plane with emphasis on avoiding jump phenomena.

### 2 Model and equations of motion

The model we study, as shown in Fig. 1, comprises a rigid body,  $\mathcal{B}$ , containing a rigid axisymmetric rotor,  $\mathcal{R}$ , and a mass particle  $\mathcal{P}$ , which is constrained to move parallel to the unit vector  $\hat{\mathbf{n}}$  fixed in  $\mathcal{B}$ . We choose a body frame such that the origin  $\mathcal{O}$  is the system mass center and the body frame axes  $\hat{\mathbf{b}}_i$  are system principal axes when  $\mathcal{P}$  is in its rest position ( $x^* = 0$ ). The vector  $\hat{\mathbf{n}}$  is parallel to  $\hat{\mathbf{b}}_1$ , which is the nominal-spin axis for the spacecraft. The particle is connected to a linear spring and has linear damping. The rotor spin-axis is in the  $\hat{\mathbf{a}}$  direction, parallel to the  $\hat{\mathbf{b}}_1$  axis. All vectors and tensors are expressed with respect to the body frame. This configuration is a reasonable model for a dual-spin spacecraft with a “ball-in-tube” type precession damper. It also can model any spacecraft with a single momentum wheel and a similar damper [14]. In a more general sense, the damper properties may be adjusted to model a flexible appendage attached to the rigid body.

The equations of motion are developed by Hughes [7] in dimensional form using a Newton–Euler approach. The system linear and angular momenta are denoted  $\mathbf{p}$  and  $\mathbf{h}$ , respectively. The linear momentum of the damper mass in the  $\hat{\mathbf{n}}$  direction is  $p_n$  and the relative displacement and velocity of the damper mass

in the  $\hat{\mathbf{n}}$  direction are  $x$  and  $\dot{x}$ . The position vector from  $\mathcal{O}$  to  $\mathcal{P}$  is  $\mathbf{r}_p = \mathbf{b} + x\hat{\mathbf{n}}$  where  $\mathbf{b}$  is a vector from  $\mathcal{O}$  to the undeformed position of the damper mass. The angular velocity of the body frame with respect to the inertial frame is  $\boldsymbol{\omega}$ . The origin of the body frame, point  $\mathcal{O}$ , has velocity  $\mathbf{v}_o$ . The rotor angular momentum component along the rotor axis of symmetry relative to the platform is  $\mathbf{h}_s = I_s\boldsymbol{\omega}_s\hat{\mathbf{a}} = h_s\hat{\mathbf{a}}$ . The symbol  $I_s$  denotes the rotor axial moment of inertia and  $\boldsymbol{\omega}_s$  is the rotor angular speed relative to the platform. The rotor is subject to axial torque  $g_a$  applied by the platform. The absolute axial rotor angular momentum is  $\mathbf{h}_a = I_s\hat{\mathbf{a}}^T\boldsymbol{\omega} + \mathbf{h}_s = I_s(\hat{\mathbf{a}}^T\boldsymbol{\omega} + \boldsymbol{\omega}_s)$ . The mass of the damper particle is  $m_d$  and the total system mass is  $m$ . The system inertia matrix is  $J$ , which depends on  $x$ . For  $x = 0$ , the moment of inertia is denoted  $I = \text{diag}(I_1, I_2, I_3)$ . The spring has stiffness  $k$  and the damper has damping coefficient  $c$ . The external force and moment are  $\mathbf{f}$  and  $\mathbf{g}$ .

We non-dimensionalize the equations using a characteristic length, mass, and time. To clarify the notation, a  $*$  superscript denotes the dimensional form of each parameter or variable, whereas the  $*$  is omitted once each is non-dimensionalized. The characteristic quantities selected are length =  $\sqrt{\text{tr}I^*/m^*}$ , mass =  $m^*$ , and time =  $\text{tr}I^*/h^*$ . The trace of the dimensionless inertia matrix is unity,  $\text{tr}I = 1$ , and, in the torque-free case, the dimensionless angular momentum vector has unit length,  $\mathbf{h}^T\mathbf{h} = 1$ .

The dimensionless equations of motion are

$$\dot{\mathbf{p}} = -\boldsymbol{\omega}^\times \mathbf{p} + \mathbf{f} \tag{1}$$

$$\dot{\mathbf{h}} = -\boldsymbol{\omega}^\times \mathbf{h} - \mathbf{v}_o^\times \mathbf{p} + \mathbf{g} \tag{2}$$

$$\dot{h}_a = g_a \tag{3}$$

$$\dot{p}_n = m_d\boldsymbol{\omega}^T\hat{\mathbf{n}}^\times[\mathbf{v}_o - (\mathbf{b} + x\hat{\mathbf{n}})^\times\boldsymbol{\omega}] - cy - kx \tag{4}$$

$$\dot{x} = y \tag{5}$$

The superscript  $\times$  denotes the skew-symmetric matrix form of a vector [7]. The system momenta may be expressed in terms of the system velocities as

$$\mathbf{p} = \mathbf{v}_o - m_dx\hat{\mathbf{n}}^\times\boldsymbol{\omega} + m_dy\hat{\mathbf{n}} \tag{6}$$

$$\mathbf{h} = J\boldsymbol{\omega} + m_dx\hat{\mathbf{n}}^\times\mathbf{v}_o + m_dy\mathbf{b}^\times\hat{\mathbf{n}} + I_s\boldsymbol{\omega}_s\hat{\mathbf{a}} \tag{7}$$

$$h_a = I_s(\hat{\mathbf{a}}^T\boldsymbol{\omega} + \boldsymbol{\omega}_s) \tag{8}$$

$$p_n = m_d(\hat{\mathbf{n}}^T\mathbf{v}_o - \hat{\mathbf{n}}^T\mathbf{b}^\times\boldsymbol{\omega} + y) \tag{9}$$

and the inertia matrix is

$$J = I + m_d[(2x\mathbf{b}^T\hat{\mathbf{n}} + x^2)\mathbf{1} - x(\mathbf{b}\hat{\mathbf{n}}^T + \hat{\mathbf{n}}\mathbf{b}^T) - x^2\hat{\mathbf{n}}\hat{\mathbf{n}}^T] \tag{10}$$

where  $\mathbf{1}$  is the identity matrix.

We reduce the order of the system equations by several simplifying assumptions consistent with the intention of studying the free motion of the damped gyrostat. Assuming that the external force is  $\mathbf{f} = 0$ , linear momentum is constant, and without loss of generality, we set  $\mathbf{p} = 0$ . Assuming the external torque is  $\mathbf{g} = 0$ , angular momentum is constant. We also assume that  $g_a = 0$  and treat  $h_a$  as a bifurcation parameter instead of as a dynamic variable. With these assumptions, we can write the velocity and angular velocity as:

$$\mathbf{v}_o = m_dx\hat{\mathbf{n}}^\times\boldsymbol{\omega} - m_dy\hat{\mathbf{n}} \tag{11}$$

$$\boldsymbol{\omega} = K^{-1}\mathbf{m} \tag{12}$$

where

$$K = I - I_s\hat{\mathbf{a}}\hat{\mathbf{a}}^T + m_d[2x\mathbf{b}^T\hat{\mathbf{n}}E - x(\mathbf{b}\hat{\mathbf{n}}^T + \hat{\mathbf{n}}\mathbf{b}^T) - m'_dx^2\hat{\mathbf{n}}^\times\hat{\mathbf{n}}^\times] \\ \mathbf{m} = \mathbf{h} - h_a\hat{\mathbf{a}} - m_dy\mathbf{b}^\times\hat{\mathbf{n}} \\ m_dy = \frac{p_n + m_d\hat{\mathbf{n}}^T\mathbf{b}^\times K^{-1}(\mathbf{h} - h_a\hat{\mathbf{a}})}{m'_d + m_d\hat{\mathbf{n}}^T\mathbf{b}^\times K^{-1}\mathbf{b}^\times\hat{\mathbf{n}}}$$

Here we have defined  $m'_d = 1 - m_d$ .

Eliminating the velocities from the equations of motion reduces the system to five scalar equations in  $\mathbf{h}$ ,  $p_n$ , and  $x$ :

$$\dot{\mathbf{h}} = \mathbf{h}^\times K^{-1}\mathbf{m} \tag{13}$$

$$\dot{p}_n = -m_d\mathbf{m}^T K^{-1}\hat{\mathbf{n}}^\times[(+m'_dx\hat{\mathbf{n}})^\times K^{-1}\mathbf{m}] - cy - kx \tag{14}$$

$$\dot{x} = y \tag{15}$$

These equations are used in the numerical and analytical studies in this paper.

### 2.1 Stability of the nominal spin

The most useful relative equilibrium is the steady spin about the  $\hat{\mathbf{b}}_1$  axis, denoted the nominal spin. Possible

spins exist about either the  $\pm\hat{\mathbf{b}}_1$  axes, but with the natural symmetry of the problem only the  $+\hat{\mathbf{b}}_1$ -axis spin is considered. For this equilibrium, the damper is not deflected and there is no damper momentum in the  $\hat{\mathbf{n}}$  direction ( $x = p_n = 0$ ). Previous works have determined the stability conditions [6, 12]:

$$I'_1 > -\max(I_2, I_3)\lambda \tag{16}$$

$$k > -(b^2m_d^2\lambda^3)/[I_1'^2(I'_1 + I_3\lambda)] \tag{17}$$

where  $I'_1 = I_1 - I_s$  and  $\lambda = h_a - 1$ .

These conditions verify that for  $h_a = 0$  and sufficiently large spring stiffness, steady spins about the major axis are stable. These results agree with stability conditions derived for rigid bodies with the same damper mechanism [1]. Non-zero wheel momentum alters the stability conditions, but qualitatively the results are similar: for a specific damper location and wheel momentum there is a critical spring constant below which the equilibrium is unstable. A prolate gyrostat, with  $I'_1 < \min(I_2, I_3)$ , requires sufficient gyroscopic stabilization for a stable nominal spin.

### 3 Bifurcations of equilibria

Equilibrium value of  $\mathbf{h}$ ,  $h_a$ ,  $p_n$  and  $x$  are found by setting Eqs. (13)–(15) equal to zero and solving the resulting algebraic equations. Linearizing these equations about the equilibrium point, the local stability of the equilibrium is found by examining the eigenvalues of the resulting Jacobian. Multiple equilibrium solutions often exist for the same values of the system parameters. Changing key system parameters, such as  $b$ ,  $k$ , or  $h_a$  may produce significantly different equilibria. Plotting equilibrium points, while varying a system parameter generates a bifurcation diagram. Critical equilibrium points may exist where the number of equilibria changes, or bifurcates. Bifurcations are often classified by the structure of the bifurcation diagram near these bifurcation points. Many references exist on bifurcation classification and theory, including Guckenheimer and Holmes [4] and Seydel [15]. To investigate the possible relative equilibria, we start from a known equilibrium point and generate bifurcation diagrams numerically using the AUTO [3] continuation program. Specifically, we begin with the  $h_a = 0$  case and then examine the more general case.

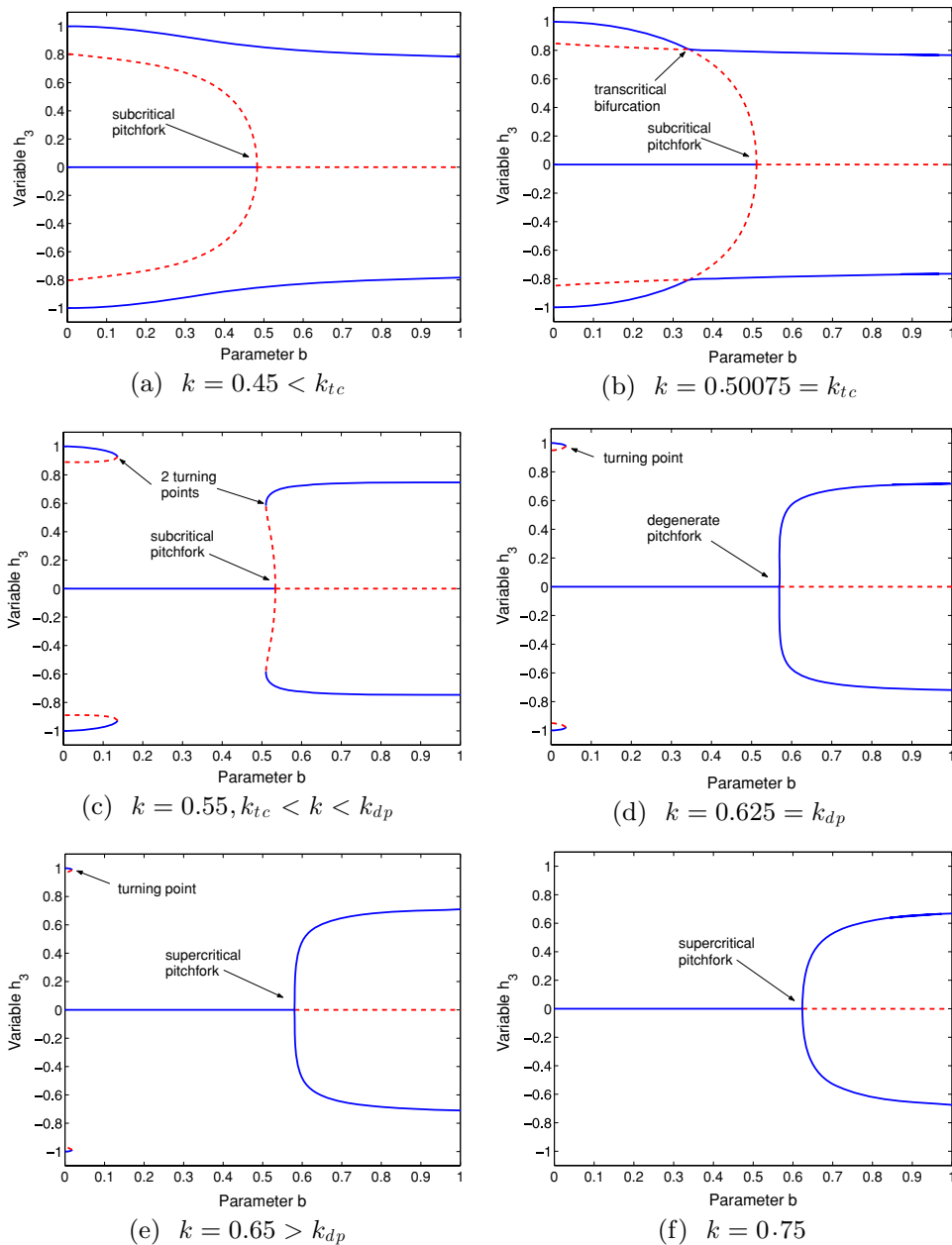


**Fig. 2** Bifurcation diagrams,  $h_3$  vs.  $b$ , for different  $k$ , illustrating selected points in  $k$ – $b$  parameter space for  $h_a = 0$ .

### 3.1 Equilibria in the $k$ – $b$ parameter plane, $h_a = 0$

In this section, we consider the constant rotor momentum case, specifically  $h_a = 0$ , and describe the possible equilibria in terms of varying  $k$  and  $b$ . Of considerable interest are the bifurcations from the nominal spin, including the off-axis branches in the  $\hat{\mathbf{b}}_1$ – $\hat{\mathbf{b}}_3$  plane. The system parameters fixed for this analysis are  $\mathbf{I} = \text{diag} [0.40, 0.28, 0.32]$ ,  $I_s = 0.04$ ,  $c = 0.1$ , and

$m_d = 0.1$ . Unless otherwise noted, we use these same parameters for all the numerical results.

Starting from the nominal equilibrium state,  $[\mathbf{h}, p_n, x] = [1, 0, 0, 0, 0]$ , we apply numerical continuation using damper location,  $b$ , as the bifurcation parameter. As shown in Fig. 2, the structure of equilibria branches changes significantly for different values of spring stiffness,  $k$ . For lower  $k$  values, the nominal spin bifurcates into a subcritical

pitchfork defined by the stability condition of Eq. (17). Additional stable, off-axis equilibria exist with  $\mathbf{h}$  in the  $\hat{\mathbf{b}}_1$ – $\hat{\mathbf{b}}_3$  plane. A significant jump from the stable nominal spin to the off-axis equilibrium is possible should the damper position be perturbed past the bifurcation point. As  $k$  increases, a transcritical bifurcation appears in the off-axis equilibria for a specific spring stiffness,  $k_{tr}$ . Increasing spring stiffness further, there are two pairs of turning points. The threshold between subcritical and supercritical pitchforks is a degenerate pitchfork with parameters  $b_{dp}$  and  $k_{dp}$ . As  $k$  slightly exceeds  $k_{dp}$ , the pitchfork is supercritical, and there is a single pair of turning points. As  $k$  increases further, there are zero turning points.

Using Eq. (17), the locus of nominal spin bifurcation points is established on the  $k$ – $b$  parameter plane. However, other turning points exist in the  $\hat{\mathbf{b}}_1$ – $\hat{\mathbf{b}}_3$  plane which may be characterized in parameter space with two-parameter continuation. The complete picture is shown in Fig. 3.

The nominal-spin bifurcation line divides the parameter space into stable and unstable nominal-spin equilibria. Superimposed on this space is the line of turning points that emanate from the degenerate pitchfork point. For fixed values of  $k$ , there are possibly 0, 1, or 2 pairs of turning points in the pitchfork branches for varying  $b$ . This  $k$ – $b$  space representation concisely expresses possible equilibria and regions in parameter space where stable nominal spins exist.

The degenerate pitchfork point is especially important to determine. This degeneracy marks the transition from subcritical to supercritical pitchfork bifur-

cations. With the associated stability changes of the pitchfork branches, the supercritical bifurcation does not exhibit the jump phenomenon of the subcritical pitchfork. Lyapunov–Schmidt has been used to determine analytical conditions for the degenerate pitchfork and the jump threshold [13]. In the general case, for  $h_a \neq 0$ , the value of  $b$  for the degenerate pitchfork is determined by

$$b_{dp}^2 = \frac{4m'_d I'_1 (I'_1 + I_3 \lambda)^2}{m_d [(3I'_1 + 2I_3 \lambda)^2 + I_1'^2 \lambda]} \tag{18}$$

Using Eq. (17), the critical spring stiffness is

$$k_{dp} = \frac{-4m_d m'_d \lambda^3 (I'_1 + I_3 \lambda)}{I_1' [I_1'^2 \lambda + (3I'_1 + 2I_3 \lambda)^2]} \tag{19}$$

For  $h_a = 0$ , the expression reduces to

$$k_{dp} = \frac{m'_d m_d}{I_1' (2I_1' - I_3)} \tag{20}$$

This relationship leads to a general design guideline for avoiding the jump phenomena. For  $k > k_{dp}$ , the pitchfork is supercritical and precludes the jump phenomenon.

### 3.2 Equilibria in the $k$ – $b$ parameter plane, $h_a \neq 0$

We expand the scope of bifurcations in the  $k$ – $b$  plane and consider the effects of rotor momentum. The natural extension of the previous section is to

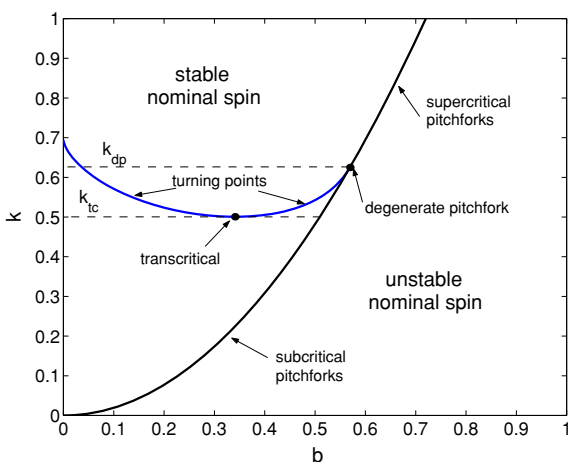


Fig. 3 Bifurcations in the  $k$ – $b$  parameter plane:  $h_a = 0$

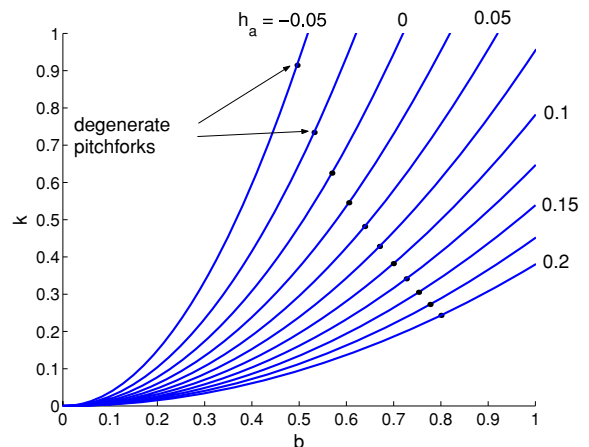
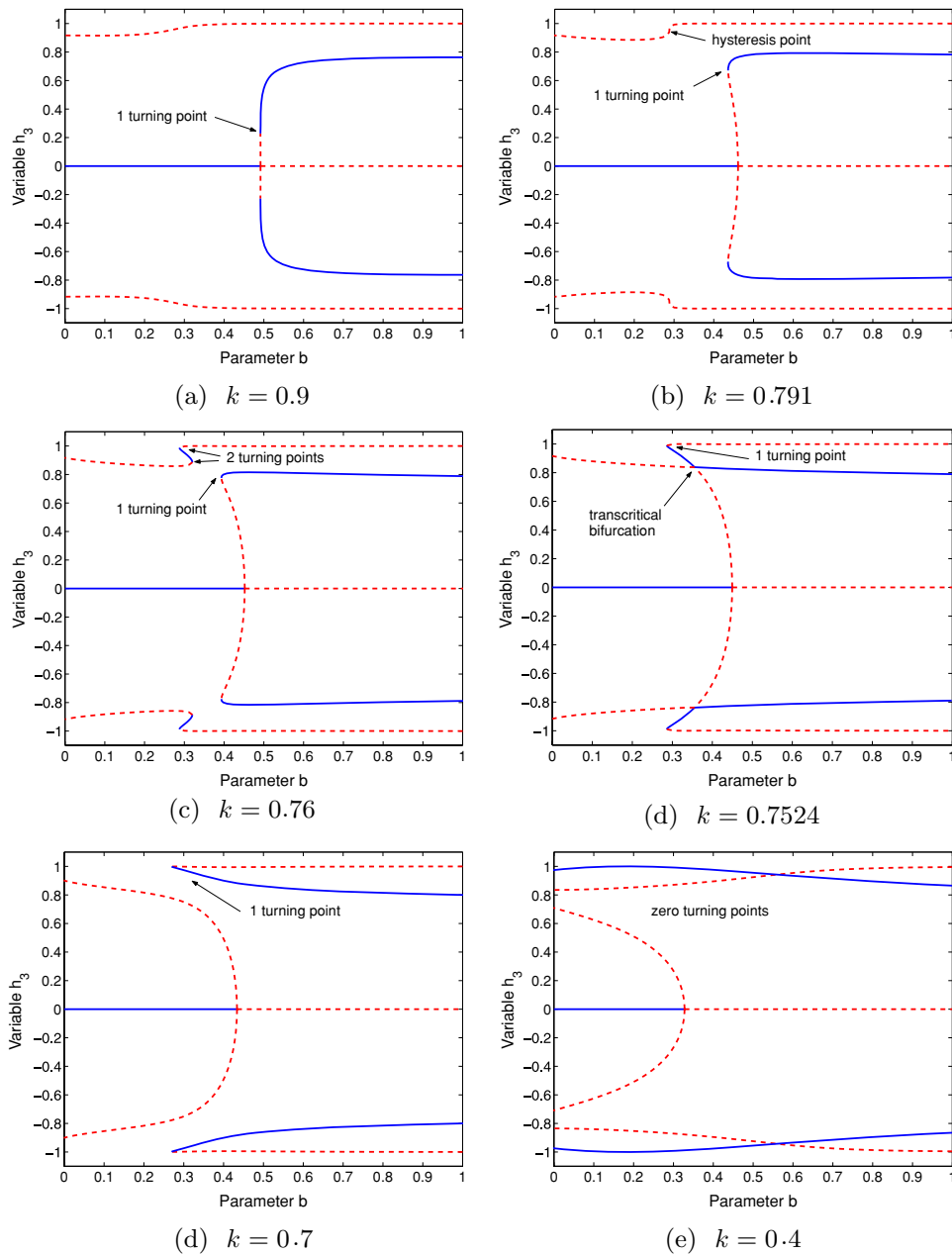


Fig. 4 Nominal-spin bifurcation branches in the  $k$ – $b$  parameter plane



**Fig. 5** Bifurcation diagrams,  $h_3$  vs.  $b$ , illustrating the evolution of equilibria and singular points as  $k$  decreases for  $h_a = -0.05$ . (a)

determine the  $k$ - $b$  parameter chart for different  $h_a$  values. Equation (17) and two-parameter continuation generate branches of singular points (pitchfork bifurcation points and turning points) in  $k$ - $b$  parameter space for different values of  $h_a$ . Not all values of  $h_a$  correspond to a bifurcation of the  $h_1 = +1$  nominal spin. Equation (17) provides an existence condition for

pitchfork bifurcations along the  $h_1 = +1$  axis:

$$1 - I'_1/I_3 < h_a < 1 \tag{21}$$

For oblate ( $I'_1 > I_3$ ) gyrostats, a pitchfork bifurcation is possible for  $h_a < 0$ , but only to this limit. Numerical studies verify that degenerate pitchforks cease to exist

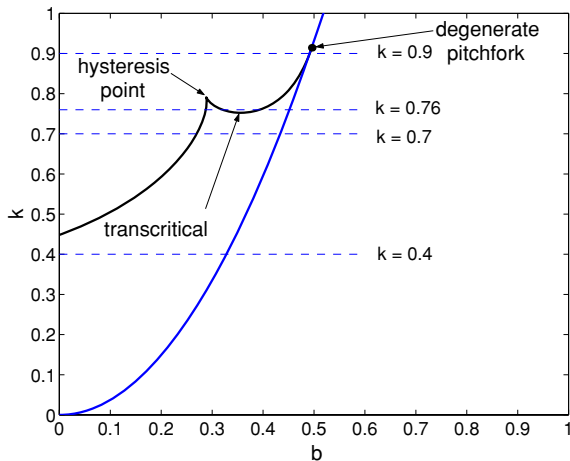


**Fig. 6** Bifurcations in the  $k$ - $b$  parameter plane:  $h_a = -0.05$

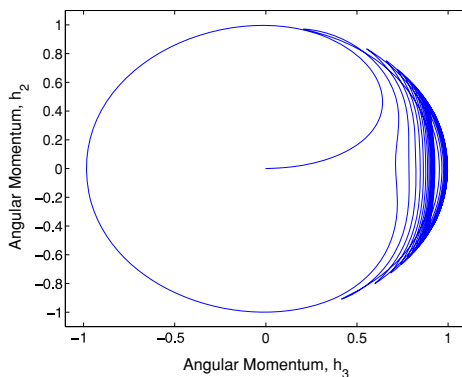
near the lower limit of Eq. (21). Therefore, we select a range of  $h_a$  values and examine how rotor momentum affects the nominal-spin bifurcation branches and the degenerate pitchfork transition.

For a range of  $h_a \in [-0.05, 0.2]$ , the nominal bifurcation branches and degenerate pitchfork points are plotted in Fig. 4. Recalling that points in parameter space above each line, toward higher values of  $k$ , represent stable nominal spins, we conclude that increasing rotor momentum creates a larger region of stable nominal spins. Since greater rotor momentum should more strongly stabilize the nominal spin of like sense (positive), this result agrees with intuition. What we also see in Fig. 4 is that for increasing rotor momentum, the degenerate pitchfork point is affected. For a

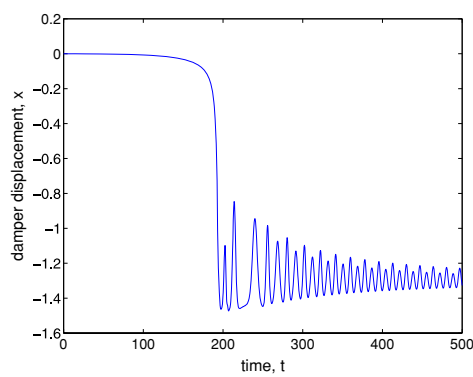
given damper position, the transition to a supercritical pitchfork occurs for a softer spring stiffness.

We look more closely at the bifurcation branches, including the turning points in the  $\hat{\mathbf{b}}_1$ - $\hat{\mathbf{b}}_3$  plane, using two-parameter continuation. We use numerical continuation to produce  $h_3$ - $b$  bifurcation diagrams for  $h_a = -0.05$  and different values of  $k$ , as shown in Fig. 5. The corresponding parameter chart in  $k$ - $b$  space is Fig. 6.

Due to the symmetry of the bifurcation diagrams, we only describe the equilibria for  $h_3 > 0$ . Figure 5(a), for  $k = 0.9$ , includes a separate, continuous off-axis branch of equilibria, with a single turning point in the nearly degenerate pitchfork. For  $k = 0.76$ , Fig. 5(c) shows that the separate off-axis branch includes two turning points that mark the ends of a stable off-axis branch, whereas the pitchfork has a single turning point. Between Fig. 5(a) and (c), there is a critical value of  $k$  where a singular point first appears in the separate off-axis branch as an inflection point, seen in Fig. 5(b). This critical value is  $k = 0.791$ , and the inflection point corresponds to a discontinuity in the  $k$ - $b$  parameter chart (Fig. 6). This point is called a cusp, or hysteresis point. The region of parameter space near the cusp may have 0, 1, or 2 singular points, not including the nominal-spin bifurcation. Figure 5 illustrates the evolution of these turning points for a range of  $k$ . The transcritical bifurcation occurs for  $k = 0.7524$ . The range of possible equilibria is concisely and completely described in  $k$ - $b$  parameter space by Fig. 6. The cusp in the  $k$ - $b$  parameter space only occurs for  $h_a < 0$ . For  $h_a > 0$ , the  $k$ - $b$  parameter chart resembles the  $h_a = 0$  case.



(a)  $h_2$  vs.  $h_3$



(b)  $x$  vs. time

**Fig. 7** Simulation of jump phenomena from a nominal spin. For  $h_a$  slightly lower than the nominal-spin bifurcation value, the system jumps to a off-axis equilibrium state

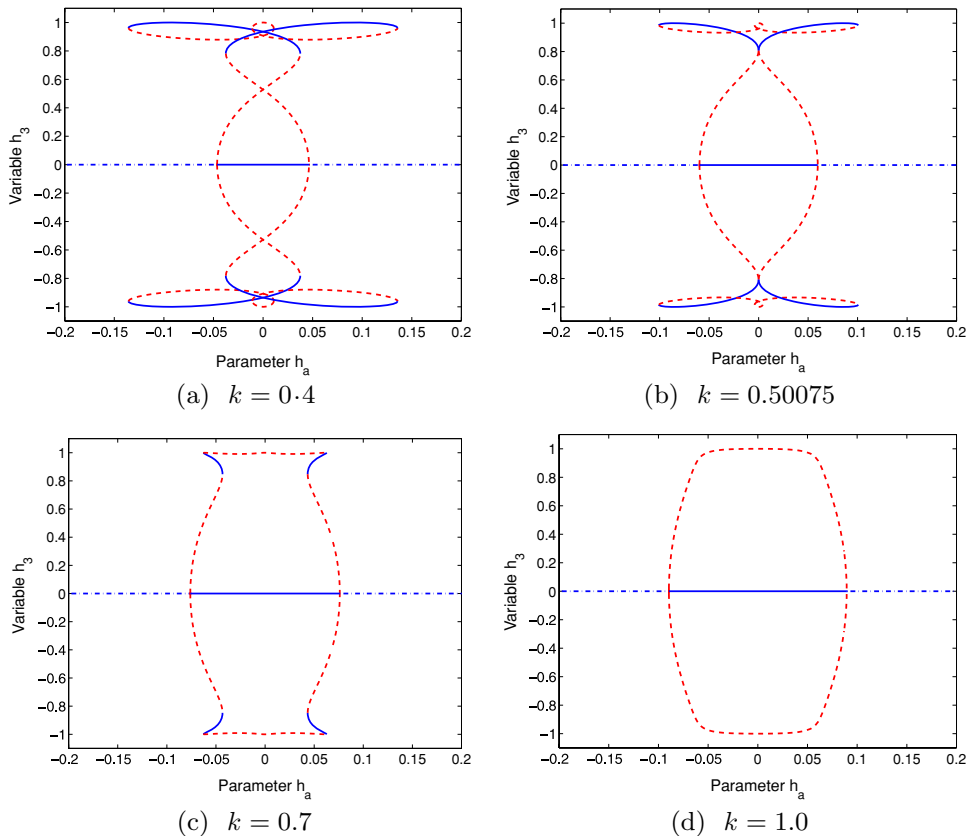


**Fig. 8** Bifurcation diagrams,  $h_3$  vs  $h_a$ , illustrating the evolution of equilibria and singular points as  $k$  increases for  $b = 0.33$

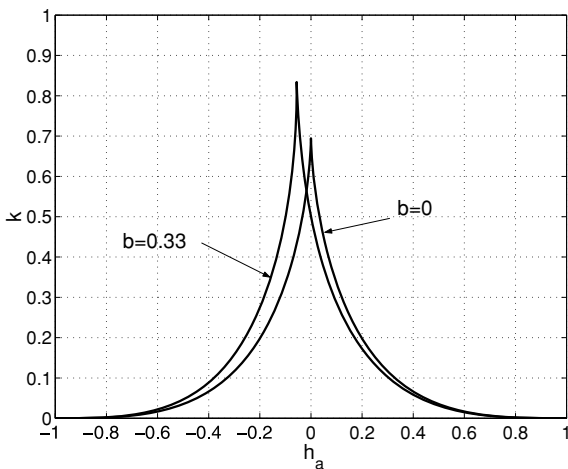


**Fig. 9** Bifurcation branches in the  $k-h_a$  parameter plane:  $b = 0$  and  $b = 0.33$

### 3.3 Equilibria in the $k-h_a$ parameter plane

We focus on the  $k-h_a$  parameter plane and identify the equilibria in the  $\hat{\mathbf{b}}_1-\hat{\mathbf{b}}_3$  plane. The degenerate pitchfork, occurring in  $h_3-b$  bifurcation diagrams, is

also found in  $h_3-h_a$  bifurcation diagrams. These degenerate points are related to the existence of stable off-axis branches of equilibria, and are therefore of practical importance. In the previous section, the likelihood of the damper position changing, and thereby destabilizing the equilibrium, seemed unlikely. By comparison, the rotor momentum seems much more vulnerable to perturbation and the resulting loss of stability.

If the nominal-spin bifurcation point is supercritical, then nominal spins are stable for  $h_a$  greater than the bifurcation value. A credible design point would be to operate on this stable nominal branch, but if for some reason rotor momentum were lost, the system would be perturbed to another stable equilibrium condition. This departure can be a significant jump: using simulation we show that the unstable nominal spin is attracted to an off-axis equilibrium, with  $x \neq 0$ , as shown in Fig. 7.

Figure 8(a)–(d) show how the stable off-axis branches of equilibria consist of branches between two turning points, and these branches ultimately converge as  $k$  increases. Note that in these figures we include both

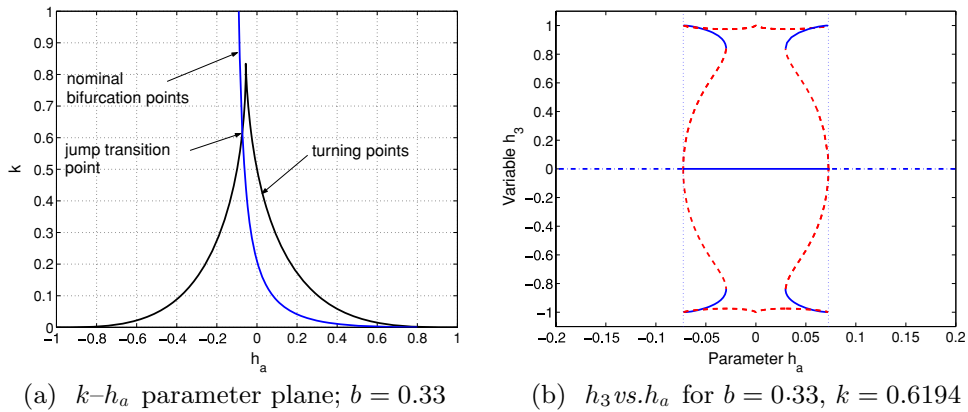


**Fig. 10** Transition of jump phenomena for stable off-axis equilibria

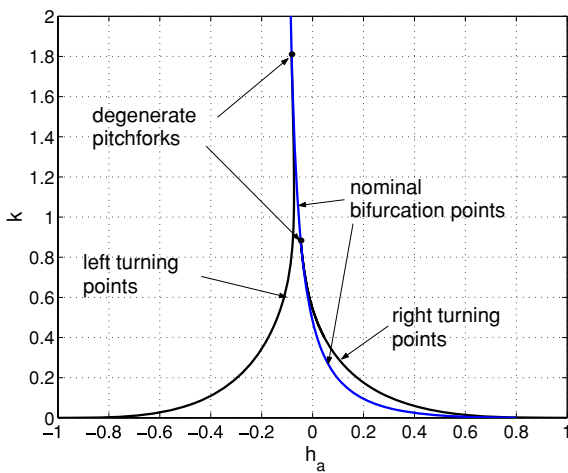


**Fig. 11** Bifurcations in the  $k-h_a$  parameter plane:  $b = 0.5$

$h_1 = \pm 1$  branches of nominal-spin equilibria, with the dash-dot line illustrating a stable and unstable branch co-existing on the  $h_3 = 0$  axis. The  $h_a = 1$  branch is unstable for lower  $h_a$  values and becomes stable at the pitchfork bifurcation point.

We use two-parameter continuation to trace these off-axis turning points in parameter space and establish the hysteresis point where they converge. However, we will also show that these two turning points do not necessarily converge to a hysteresis point, but may converge on the nominal bifurcation point, creating a degenerate pitchfork.

Using the same system parameters as before, we first consider the  $k-h_a$  parameter charts of the turning points for  $b = 0$  and  $b = 0.33$  (Fig. 9). Both cases generate a cusp in parameter space. This point defines the point in parameter space where the stable off-axis branch disappears. For  $k > k_{\text{cusp}}$ , nominal-spin

equilibria are the only possible stable spins. As with earlier examples of cusps in parameter space, there can be 0, 1, or 2 pairs of turning points depending on the region of parameter space.

The absence of stable off-axis branches means if rotor momentum is lost, an  $h_1 = +1$  spin will become an  $h_1 = -1$  spin. However, this jump may also occur for a small, stable off-axis branch. If the stable off-axis branch only occurs for  $h_a$  greater than the bifurcation point, the jump will behave as if there were no stable off-axis branches. To find this transition in parameter space, we plot the turning point branches along with the locus of nominal bifurcation points in Fig. 10(a). The key point is where the two branches of singular points cross. For  $k$  greater than this critical value, stable off-axis branches exist, but only for  $h_a$  greater than the nominal bifurcation point. For  $k$  less than this jump transition value, a nominal equilibrium perturbed to a lower rotor momentum will jump to the corresponding off-axis equilibrium point. For this example, the two bifurcation branches cross at  $k = 0.6194$ , which is used to generate Fig. 10(b).

As  $b$  increases further, there is no longer a cusp, but the turning points ultimately merge with the nominal bifurcation branch, resulting in a degenerate pitchfork. These degenerate points are the same in parameter space as those previously described. The degenerate pitchfork is identified by Equation (18), and yields a critical value for  $\pm b$  for a given value of  $\lambda$ . Due to the symmetry of the problem, the  $-b$  case is not separately discussed. For the  $k-h_a$  perspective in parameter space, a given value of  $b$  yields two distinct values of  $h_a$ . For a given value of  $b$ , Equation (18) produces real values of  $h_a$  when

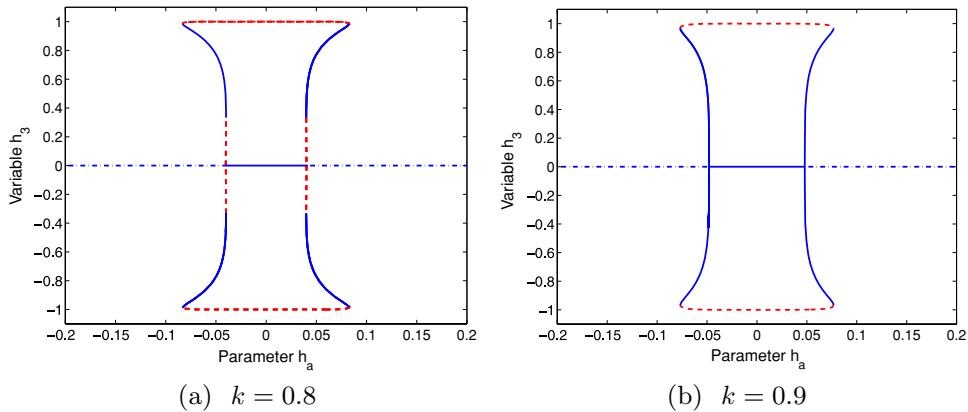


**Fig. 12** Bifurcation diagrams,  $h_3$  vs.  $h_a$ , near the first degenerate pitchfork for  $b = 0.5$ . As  $k$  increases from  $0.8 \rightarrow 0.9$ , the turning points on off-axis branches converge with the nominal-spin

bifurcation point, forming degenerate pitchforks. Another set of limit points remains in the off-axis branches of equilibria

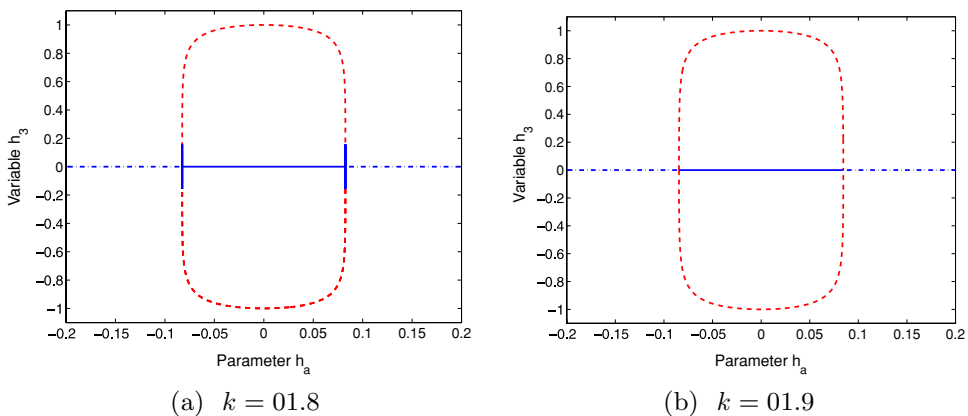


**Fig. 13** Bifurcation diagrams,  $h_3$  vs.  $h_a$ , near the second degenerate pitchfork for  $b = 0.5$ . As  $k$  increases from  $1.8 \rightarrow 1.9$ , the final set of turning points on the off-axis branches converge with the nominal-spin bifurcation point, forming degenerate pitchforks

$$b^2 > \frac{16m'_d(I'_1 - I_3)}{m_d(I'_1 + 24I_3)} \tag{22}$$

For the parameters of the preceding example, the critical value of the damper location is  $b = 0.4788$ . For  $b$  below this threshold, a cusp appears in the parameter chart as the two turning points converge for increasing  $k$ , seen in Fig. 9. For  $b$  above this threshold there are two distinct degenerate pitchfork bifurcation points in parameter space where the turning points converge with the nominal bifurcation branch. Figure 11 shows the bifurcation branches for both turning points of the stable off-axis branch. Instead of converging, they move toward and combine with the branch of nominal bifurcation points. The  $k$  values of the two degenerate points are denoted  $k_{dg1}$  and  $k_{dg2}$ .

Figures 12–13 show the bifurcation diagrams including the pitchforks before and after the degenerate points. The first (lower) turning point converges with the nominal bifurcation point first. For  $k_{dg1} < k < k_{dg2}$ , the pitchfork branches are stable, precluding any jump phenomena. The second turning point becomes degenerate for a higher value of spring stiffness,  $k = k_{dg2}$ . Increasing  $k$  further results in entirely unstable off-axis equilibria, and therefore the nominal spin is the only stable equilibrium.

### 4 Summary

We used two-parameter continuation and Lyapunov–Schmidt reduction to characterize bifurcations in  $k$ – $b$ – $h_a$  parameter space. Using two-parameter continuation and the stability criterion for the nominal

spin, we produce parameter charts that describe a set of possible singular points in parameter space. We identify subcritical, degenerate, and supercritical pitchfork bifurcations of the nominal-spin equilibrium. We also determine branches of turning points in the  $\hat{\mathbf{b}}_1$ – $\hat{\mathbf{b}}_3$  plane and their relationship with the nominal-spin equilibria. Special cases are identified, including a transcritical bifurcation and cusps in parameter space. Lyapunov–Schmidt reduction generates an analytical relationship between  $k$ ,  $b$ , and  $h_a$  that identifies a degenerate pitchfork bifurcation of the nominal spin equilibrium. The degenerate pitchforks are seen in several perspectives, including the  $h_3$ – $b$  and  $h_3$ – $h_a$  bifurcation diagrams. For larger values of  $b$ , two degenerate pitchfork points may occur in the  $k$ – $h_a$  parameter space. The degenerate point marks the transition between subcritical and supercritical pitchforks, and provides a design criterion to avoid jump phenomena.

**Acknowledgements** The first author was supported by the Air Force Institute of Technology’s Civilian Institutions program for Air Force Academy Faculty Preparation. The second author was supported by the Air Force Office of Scientific Research and the National Science Foundation.

## References

- Chinnery, A.E., Hall, C.D.: Motion of a rigid body with an attached spring-mass damper. *J. Guid. Control Dynam.* **18**(6), 1404–1409 (1995)
- Cloutier, G.J.: Stable rotation states of dual-spin spacecraft. *J. Spacecraft Rockets* **5**(4), 490–492 (1968)
- Doedel, E.J., Champneys, A.R., Fairgrieve, T.F., Kuznetsov, Y.A., Sandstede, B., Wang, X.: AUTO 97: continuation and bifurcation software for ordinary differential equations. Concordia University, Montreal, Canada (1998)
- Guckenheimer, J., Holmes, P.: *Nonlinear Oscillations, Dynamical Systems, and Bifurcations of Vector Fields*. Springer-Verlag, New York (1983)
- Hall, C.D.: Spinup dynamics of gyrostats. *J. Guid. Control Dynam.* **18**(5), 1177–1183 (1995)
- Hall, C.D.: Momentum transfer dynamics of a gyrost with a discrete damper. *J. Guid. Control Dynam.* **20**(6), 1072–1075 (1997)
- Hughes, P.C.: *Spacecraft Attitude Dynamics*. John Wiley and Sons, New York (1986)
- Landon, V.D., Stewart, B.: Nutational stability of an axisymmetric body containing a rotor. *J. Spacecraft Rockets* **1**(6), 682–684 (1964)
- Likins, P.W.: Attitude stability criteria for dual spin spacecraft. *J. Spacecraft Rockets* **4**(12), 1638–1643 (1967)
- Likins, P.W.: Spacecraft attitude dynamics and control—a personal perspective on early developments. *J. Guid. Control Dynam.* **9**(2), 129–134 (1986)
- Mingori, D.L.: Effects of energy dissipation on the attitude stability of dual-spin satellites. *AIAA J.* **7**(1), 20–27 (1969)
- Sandfry, R.A.: Equilibria of a gyrost with a discrete damper. Ph.D. thesis, Virginia Polytechnic Institute and State University (2001)
- Sandfry, R.A., Hall, C.D.: Relative equilibria of a prolate gyrost with a discrete damper. *J. Astronaut. Sci.* **50**(4), 367–387 (2002)
- Schneider, C.C., Likins, P.W.: Nutation dampers vs precession dampers for asymmetric spinning spacecraft. *J. Spacecraft Rockets* **10**(3), 218–222 (1973)
- Seydel, R.: *Practical Bifurcation and Stability Analysis*, 2nd edn. Springer-Verlag, New York (1994)